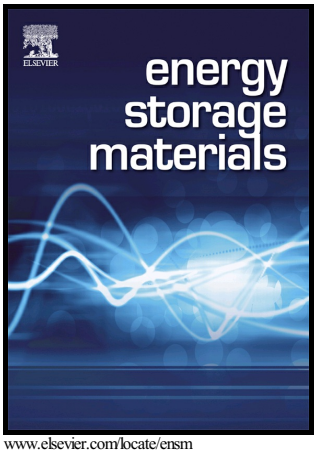

www.elsevier.com/locate/ensm

Sc and Nb Dopants in $SrCoO_3$ Modulate Electronic and Vacancy Structures for Improved Water Splitting and SOFC Cathodes

Hassan A. Tahini, Xin Tan, Wei Zhou, Zhonghua Zhu, Udo Schwingenschlögl, Sean C. Smith

PII: S2405-8297(16)30226-4
DOI: http://dx.doi.org/10.1016/j.ensm.2017.01.005
Reference: ENSM117

To appear in: *Energy Storage Materials*

Received date: 17 August 2016
Revised date: 18 December 2016
Accepted date: 11 January 2017

Cite this article as: Hassan A. Tahini, Xin Tan, Wei Zhou, Zhonghua Zhu, Udo Schwingenschlögl and Sean C. Smith, Sc and Nb Dopants in $SrCoO_3$ Modulat Electronic and Vacancy Structures for Improved Water Splitting and SOFC C a t h o d e s , *Energy Storage Materials* http://dx.doi.org/10.1016/j.ensm.2017.01.005

Sc and Nb Dopants in $SrCoO_3$ Modulate Electronic and Vacancy Structures for Improved Water Splitting and SOFC Cathodes

Hassan A. Tahini[1], Xin Tan[1], Wei Zhou[2], Zhonghua Zhu[3], Udo Schwingenschlögl[4], Sean C. Smith[1*]

[1]*Integrated Materials Design Centre (IMDC), School of Chemical Engineering, UNSW Australia, Sydney, NSW 2052, Australia*

[2]*State Key Laboratory of Materials-Oriented Chemical Engineering, College of Chemistry & Chemical Engineering, Nanjing Tech University, No. 5 Xin Mofan Road, Nanjing 210009, P.R. China.*

[3]*School of Chemical Engineering, The University of Queensland, St. Lucia, Queensland 4072, Australia.*

[4]*Physical Science & Engineering Division, KAUST, Thuwal 23955-6900, Kingdom of Saudi Arabia*

***Corresponding Author. sean.smith@unsw.edu.au**

Abstract

$SrCoO_3$ is a promising material in the field of electrocatalysis. Difficulties in synthesising the material in its cubic phase have been overcome by doping it with Sc and Nb ions [*Mater. Horiz.* **2015**, *2*, 495–501]. Using ab initio calculations and special quasi random structures we undertake a systematic study of these dopants in order to elucidate the effect of doping on electronic structure of the $SrCoO_3$ host and the formation of oxygen vacancies. We find that while the overall electronic structure of $SrCoO_3$ is preserved, increasing the Sc fraction leads to a decrease of electrical conductivity, in agreement with earlier experimental work. For low Sc and Nb doping fractions we find that the oxygen vacancy formation increases relative to undoped $SrCoO_3$. However, as the dopants concentration is increased the vacancy formation energy drops significantly, indicating a strong tendency to accommodate high concentration

of oxygen vacancies and hence non-stoichiometry. This is explained based on the electronic instabilities caused by the presence of Sc ions which weakens the B-O interactions as well as the increased degree of electron delocalization on the oxygen sublattice. Sc dopants also shift the p-band centre closer to the Fermi level, which can be associated with experimentally reported improvements in oxygen evolution reactions. These findings provide crucial baseline information for the design of better electrocatalysts for oxygen evolution reactions as well as fuel-cell cathode materials.

KEYWORDS: perovskite; transition metal; electrocatalyst; SOFC; DFT; vacancies,

1. Introduction

Energy generation and storage with a low carbon footprint is necessary to mitigate the undeniable effect that fossil fuel utilization has on the environment. Renewable energy in the form of solar and wind energy transformed into electricity can be used in conjuncture with electrocatalysis in electrolyzers to generate hydrogen which can be stored and utilized as a fuel [1,2].

For this to be realized, it is necessary to find low cost, efficient and easily processable materials which exhibit the necessary catalytic activity to be used for water splitting and in fuel cells. Perovskites have emerged as a key candidate material in the field of electrocatalysis, given their moderate cost and good activity, which can in some cases come close to and even surpasses that of noble metals [3–5]. The other advantage perovskites offer is the capacity to tune their properties by modest changes to the chemical constituents. Issues remain regarding their long term stability and the relatively high operating temperature (900~1200 C) needed in order to achieve adequate transport of electrons and ions in solid

oxide fuel cells (SOFC).[6] Also the high overpotentials associated with oxygen evolution and reduction reactions are still a major obstacle to fully realize water splitting on a commercial scale.

Among the numerous possible perovskites, $SrCoO_3$ has emerged as a desirable electrode material due to its oxygen non-stoichiometry and superior redox capabilities of the Co ions [7–11]. The remarkable redox ability of Co has been demonstrated in barium strontium cobalt iron oxide ($Ba_{0.5}Sr_{0.5}Co_{0.8}Fe_{0.2}O_{3-\delta}$) which has been widely studied as a cathode material for SOFCs [12–14]. Recently, Suntivitch et al [15]. demonstrated that BSCF has one of the lowest overpotentials for the oxygen evolution reactions (OER), however, the material suffers from low stability and readily amorphizes under operating conditions [16,17].

Theoretical predictions have placed $SrCoO_3$ at the top of the activity volcano plots for OER with overpotentials predicted at 0.25~0.30 eV [18,19]. Experimental work investigating the series formed by $La_{1-x}Sr_xCoO_3$ have demonstrated an improved activity for higher Sr fraction [11]. This was recently explained by Cheng et al. [20] on the basis that Sr substitutions straightens the Co-O-Co bonds and further oxidizes Co^{3+} increasing the overlap between O 2p and Co 3d bands, which enhances the electronic conductivity. In this work we examine the effect of Sc and Nb dopants inspired by the recent demonstration that $SrSc_xNb_yCo_{1-x-y}O_3$ can exhibit low overpotentials and high stability under OER conditions. We show that low doping fractions can favour OER due to the suppression of oxygen vacancies, which is reflected in higher oxygen stoichiometries. High Sc content, on the other hand, leads to a large decrease in the oxygen vacancy formation energy and can impact the crystallinity of the doped structure.

2. Methodology

Our calculations are based on VASP's implementation [21] of density functional theory with the projector augmented waves method [22] to treat core and valence electrons. The Sr ($4s^2 4p^6 5s^2$), Sc ($3s^2 3p^6 4s^2 3d^1$), Nb ($4p^6 5s^1 4d^4$) Co ($3p^6 4s^2 3d^7$) and O ($2s^2 2p^4$) electrons were treated as valence. The generalized gradient approximation with the PBEsol [23] parameterization was used to describe the exchange-correlation, which is more suited to describe solids' properties [20,24–27]. Plane waves with kinetic energy cutoff of 500 eV were used to expand the wavefunctions, with larger cutoff of 600 eV leading to changes of ~ 0.05 eV in the formation energies. Energies were converged with a $1x10^{-5}$ eV tolerance and forces were optimized until they change by no more than $1x10^{-2}$ eV/Å.

To mimic the random distribution of the B-site dopants, special quasirandom structures (SQS) were used. These were generated using the Monte Carlo SQS tool within the Alloy Theoretical Automated Toolkit (ATAT) [28]. The SQS method was used as an efficient and reliable tool in modelling disorder in a number of oxides and perovskites.[29–32] Electronic interactions between ions are studied using the crystal orbital Hamilton population (COHP) as implemented in the LOBSTER code [33,34].

Vacancies are modelled using a 135 atom supercell which is large enough to reduce image-image interactions due to periodic boundary conditions. Based on earlier work, this supercell size was shown to be large enough to model a vacancy in the dilute limit.[35]

3. Results and Discussions

$SrSc_xNb_yCo_{1-x-y}O_3$: distributions and structures

In order to incorporate B-site Sc and Nb doping into $SrCoO_3$ that would justifiably reflect experimental structures, we relied on the use of the SQS technique to populate the B sites. The starting point was a 3x3x3 ABO_3 cell which contains 27 possible B sites. In all the models one Nb atom was always present which corresponds to a fraction of y = 0.037. The Sc

fraction x was varied between 0.037 (1 Co) and 0.222 (6 Co). The remaining sites were populated with Co atoms. The choice of these doping fractions stems from the recent work by Zhou et al. [36]. For each of the doping fractions a number of cells are generated that attempt to minimize an objective function which matches a number of correlation functions. For this we use pair and triplet correlation functions set to the 3rd and 2nd neighbour distance, respectively. The resulting structures are shown in Fig. 1.

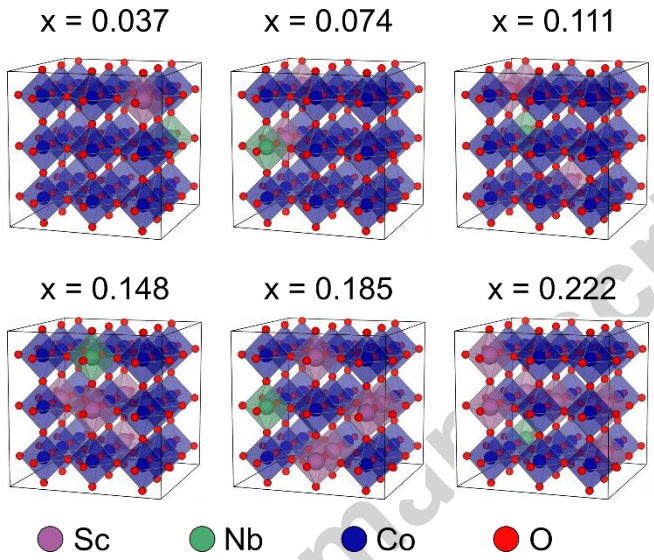

Figure 1. The 135 atom supercell used to mimic the Sc and Nb distribution in $SrSc_xNb_{0.037}Co_{0.963-x}O_3$.

This was followed by a structural relaxation for each of the configurations shown in Fig. 1. We perform this in a series of two stage relaxations: first allowing the atoms to relax and then relaxing the cell parameters (but not the shape).

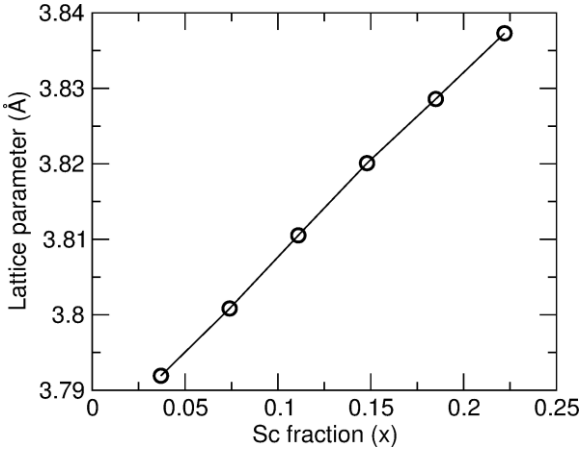

Figure 2. The relaxed cell parameter as a function of the Sc fraction. The linear behaviour is in close agreement with Vegard's law.

The effect of increasing the Sc fraction is to expand the lattice. If we ignore the effect of the small Nb doping fraction, the behaviour shown in Fig. 2 is in good agreement with the experimental work of Zeng et al. [37] who investigated Sc doping in the range of 0.02-0.2 in $SrSc_xCo_{1-x}O_3$. The effect of increasing Sc can be simply understood from Vegard's law. The calculated lattice parameter of hypothetical $SrScO_3$ is 4.08 Å while that of $SrCoO_3$ is 3.78 Å which leads to an overall similar shape similar to that shown in Fig. 2, when interpolating between the two limits.

Electronic structure of $SrSc_xNb_{0.037}Co_{0.963-x}O_3$

To help understand the electronic interactions in $SrSc_xNb_{0.037}Co_{0.963-x}O_3$ it is useful to examine the electronic interactions between Co/Sc and O. The Sc-O and Co-O interactions in $SrScO_3$ and $SrCoO_3$ are shown in Fig. 3. One can clearly see an inherent instability in the Sc-O interaction with no bonding interactions at the Fermi level and large antibonding contribution at about 3 eV below the Fermi level. On the other hand $SrCoO_3$ shows some

antibonding interactions at the Fermi level but retains a mainly bonding character which leads to an overall stable structure. In $SrNbO_3$, the interaction is mainly dominated by a strong bonding interaction. However, these bonding states are well below the Fermi level.

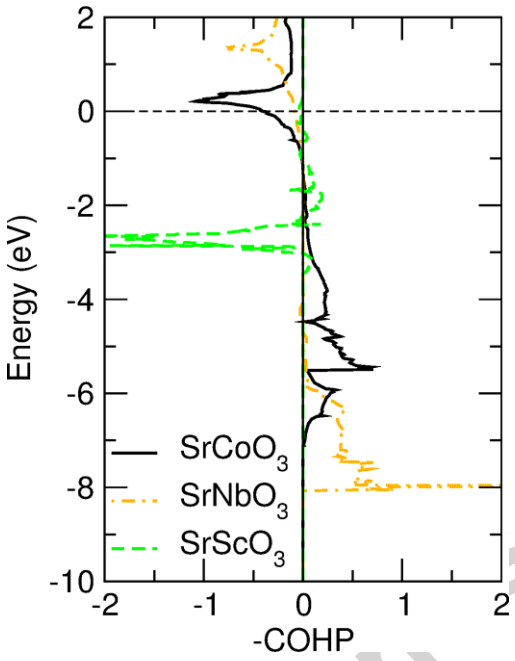

Figure 3. The COHP representation (negative and positive values correspond to antibonding and bonding interactions, respectively) of the Co-O, Nb-O and Sc-O interactions in $SrCoO_3$, $SrNbO_3$ and $SrScO_3$, respectively. SrScO3 exhibits an electronic instability while in $SrNbO_3$ Nb-O display bonding interactions between -8 to -6 eV.

The projected densities of the Co 3d and O 2p states for each of the compositions considered here are shown in Fig. 4. At low Sc fractions (x = 0.037 and 0.074) there is a strong mixing of the Co and O states in the valence band, with clear indications of hybridizations in the range of -3 to -1 eV which is characteristic of the expected degree of covalency in $SrCoO_3$. A sizable density of states occurs at the Fermi level, which is dominated mainly by the minority spin channel of the Co ions. As the Sc fraction is increased the Co 3d peak starts to diminish and clearly disappears for the Co 3d minority spin electrons in the valence band signalling a

reduction in hybridization between Co and O in agreement with previous theoretical calculations [38].

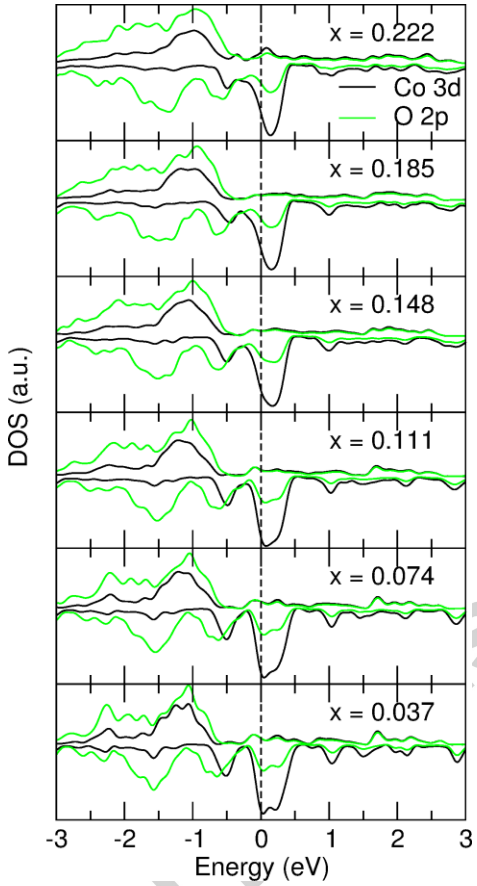

Figure 4. The PDOS evolution with Sc content showing contributions from the Co 3d and O 2p states.

Furthermore, Sc doping shifts some of the states above the Fermi level as can be seen in Fig. 4 where the Co/O peak at the Fermi level moves to higher energy. This implies an increased hole concentration and an emergence of p-type conductivity which was experimentally reported by Zeng et al. [37]. Increasing the Sc content will eventually lead to a decrease in conductivity as the Sc^{3+} have a fixed valency and would not contribute to electrical conductivity, which is expected to be mediated by a Zener double exchange process controlled by the strongly overlapping B–O–B bonds [37].

The charges on the ions where calculated using the Bader decomposition algorithm [39]. Table 1 shows the effective charges for each composition. The charges were averaged over each species and compared to the values obtained in bulk $SrCoO_3$, $SrScO_3$ and $SrNbO_3$.

Table 1. Bader charges for each species in the parent perovskite compound and at each $SrSc_xNb_{0.037}Co_{0.963-x}O_3$ composition and the corresponding lattice parameters.

		Charges					
		q_{Sr}	q_{Sc}	q_{Nb}	q_{Co}	q_O	Lattice parameter (Å)
	$SrCoO_3$	1.57	-	-	1.52	-1.03	3.78
	$SrScO_3$	1.59	1.90	-	-	-1.16	4.08
	$SrNbO_3$	1.58	-	2.27	-	-1.28	4.05
	0.037	1.57	1.88	2.61	1.47	-1.03	3.79
	0.074	1.57	1.90	2.47	1.47	-1.03	3.80
x	0.111	1.57	1.89	2.47	1.48	-1.04	3.81
	0.148	1.57	1.89	2.54	1.48	-1.05	3.82
	0.185	1.57	1.90	2.57	1.49	-1.06	3.83
	0.222	1.57	1.90	2.53	1.50	-1.06	3.84

The charge on Sr is about +1.57e which is close to the formal charge of +2e in $SrBO_3$ bulk systems. This value remains constant and shows no dependence on the values of x. Similarly the charge on Sc, which formally adopts a +3 oxidation state, remains close to the bulk value of +1.90e. Nb and Co are more flexible. Nb shows a markedly different oxidation when incorporated with Sc in $SrSc_xNb_{0.037}Co_{0.963-x}O_3$. On average Nb donates about 0.2e more electrons in $SrSc_xNb_{0.037}Co_{0.963-x}O_3$ compared with bulk $SrNbO_3$ whereas the charge on Co decreases from its bulk SrCoO3 value before increasing again as the Sc fraction is increased. In general the small charges acquired by each species is an indication of the covalent character and is typical for this type of compounds [31,32,40–42].

Oxygen vacancies $SrSc_xNb_{0.037}Co_{0.963-x}O_3$

The presence of oxygen vacancies is inevitable in oxides. They can affect electrochemical activities in catalysts and they play a pivotal role in SOFC as they mediate the oxygen ions reduction and diffusion. Here we model the oxygen vacancies by removing a neutral O atom from the SQS corresponding to a particular composition for which the formation energy is calculated as:

$$E_f(V_O) = E(V_O) - E(\text{perf}) + \frac{1}{2}[\Delta h + E(O_2)]$$

Where $E(V_O)$, $E(\text{perf})$ and $E(O_2)$ are the total energies of the defect containing supercell, perfect SQS supercell and the energy of an O_2 molecule. Δh is a correction term added to account for the well-known O_2 overbinding in DFT calculations. This value is obtained by fitting the heats of formation of a range of oxides and determining the offset from the well characterized experimentally determined heats of formation [43,44]. The oxygen overbinding correction is functional dependent. For PBEsol we find that $\Delta h = 0.9$ eV which is in good agreement with previous work [45]. The above definition of E_f corresponds to oxygen rich conditions.

Given that a defect's formation energy is dependent on its local environment we calculated the O formation for all possible configurations which were classified according to Sc-V_O-Co, Nb-V_O-Co, Sc-V_O-Sc and Co-V_O-Co. The most recurring pairs are shown in Fig. 5. It is clear from the figure that there is a spread of the formation ranging about 1 eV in some cases. In general, defects with the lowest formation energies are thermodynamically favourable, however, under experimental synthesis and operating conditions temperatures can reach 1000 K which implies that a proportion of high energy defects could become thermodynamically accessible. A configurational average could then be used to estimate the formation energy for an O vacancy in a particular B-V_O-B' configuration according to [46]:

$$\langle E_f \rangle = \frac{\sum_n E_f^n \exp(-E_f^n/k_B T)}{\sum_n \exp(-E_f^n/k_B T)} \quad (1)$$

Where $\langle E_f \rangle$ is the configuration average over the n possible configuration each with formation energy E_f^n, k_B is Boltzmann's constant and the temperature T is set to 1000 K which is a typical processing temperature for a ceramic solid state reaction and SOFC operation.[36]

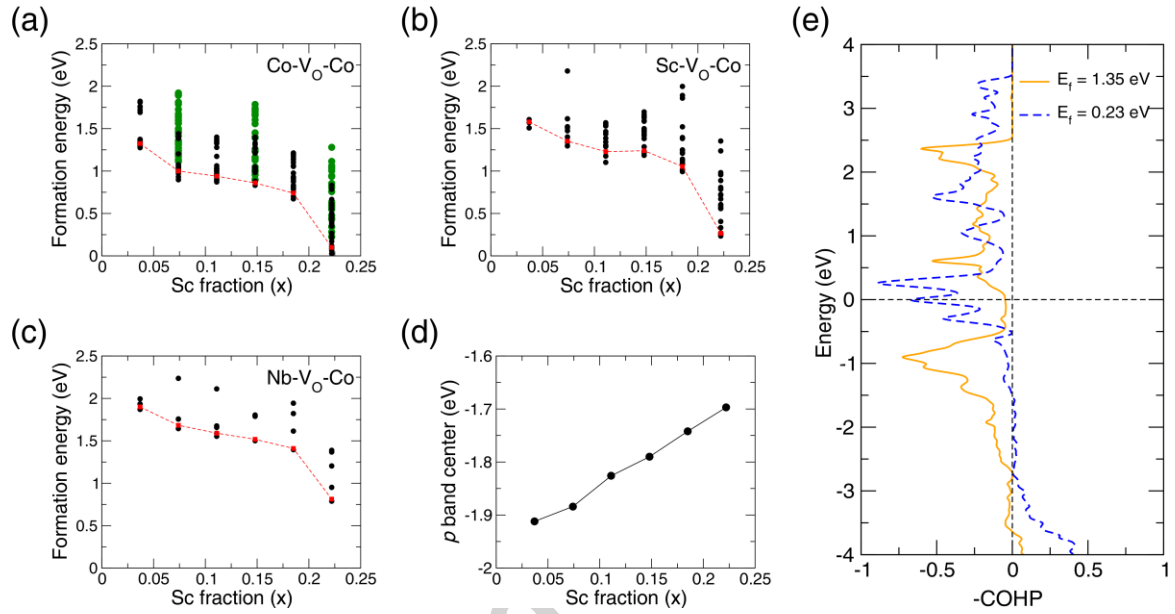

Figure 5. Oxygen vacancy formation energy for each composition x = 0.037-0.222. Each data point corresponds to a different local environment surrounding the oxygen vacancy. The local environments are classed into three major groups (a) Co-V_O-Co, (b) Sc-V_O-Co and (c) Nb-V_O-Co. The O p-band centres calculated in the defect free systems is shown in (d). The COHP interactions for the highest and lowest formation energy sites in the Sc-V_O-Co configuration at x = 0.222. Configurationally averaged oxygen vacancies are represented by red dots and are joined by a red (dashed) line. The larger green dots in (a) were obtained using GGA+U.

Starting from low Sc doping fractions (x = 0.037), oxygen vacancies adjacent to the dopant atoms have high formation energies relative to a single isolated vacancy in $SrCoO_3$ [35] which was found to be 1.26 eV in the dilute limit (1.37 eV in a 3x3x3 supercell). For instance the Nb-V_O-Co forms at 1.9 eV whereas Sc-V_O-Co forms at 1.54 eV. The increase in the vacancy formation energy is the highest in the vicinity of Nb. This is supported by experimental evidence that showed a strong correlation between Nb content and oxygen stoichiometry in $SrCoO_3$ [47].

The trends shown in Fig. 5(a)-(c) show that as the fraction of Sc is increased the average cost to form an oxygen vacancy decreases regardless of the B-V_O-B' configuration type. Two major contributions to the defect formation in a perovskite (or solids in general) are the extent of structural distortions (such as the rotations and tilting of the MO_6 octahedra in this case) and the electronic redistributions. While the formation of an oxygen vacancy causes a clear distortion in the lattice which is marked by B-O-B bond angles deviating significantly from the 180° as in the cubic case, we find that the degree of distortion is similar in all cases, i.e. at the same Sc doping fractions as well as for low and high doping fractions. Therefore, lattice distortions cannot explain the variation in formation energies. To understand this we focus on the bonding of the O atom at a given configuration. Considering the bonding/antibonding interactions of an O atom with its surrounding transition metal sites we see that the introduction of Sc species increases the antibonding contribution in the structure (Fig. 3). For instance Fig. 5(b) shows that for Sc-V_O-Co at x = 0.222 the most stable O defect has formation energy of 0.21 eV while the least favourable one occurs at 1.35 eV. Taking these two defects as an example to illustrate the effect of bonding/antibonding interactions, we consider the two O sites at these two configurations in the perfect SQS supercell for x = 0.222. We calculate the interaction of each of the O atoms with its neighbouring transition metal sites using the COHP technique as shown in Fig. 5(e). We can clearly see that the

easily-formed V_O defect has a high proportion of states at the Fermi level with a strong antibonding character. On the other hand, the high formation energy V_O defect exhibits negligible antibonding character at the Fermi level. Similarly, Nb ions show a strong bonding character in bulk $SrNbO_3$ which will lead to an increase in V_O formation energy as is the case for the considered range of x. To test the robustness of the observed trends in V_O formation energies we performed additional calculations using GGA+U ($U_{eff} = 3.3$ eV [43,48,49]) focusing on the Co-V_O-Co case. We found that while the absolute values of $E_f(V_O)$ change compared with pure PBE, the same trend holds showing a clear drop in formation energies as the Sc content is increased (see Fig. 5(a)).

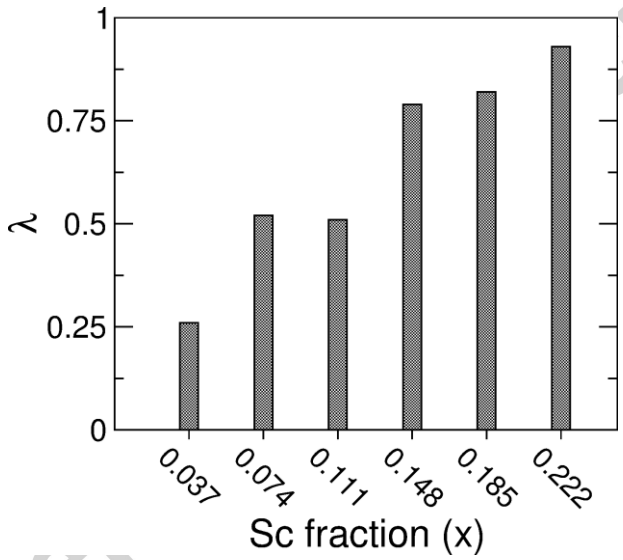

Figure 6. Electron delocalization over the oxygen sublattice for Co-V_O-Co configurations.

Oxygen vacancy formation energies were also successfully described based on the degree of charge delocalization of the electrons left behind upon the removal of an oxygen atom.[32,41,50,51] It was established that a higher degree of charge delocalization on the oxygen sublattice results in lower vacancy formation energies.[50,51]. The degree of localization (λ) was calculated using:[32]

$$\lambda = \frac{(N-1)\left(\langle q_{O,nonstoichiometric}\rangle - \langle q_{O,stoichiometric}\rangle\right)}{\langle q_{O,stoichiometric}\rangle} \quad (2)$$

Where N is the number of oxygen in the perfect reference system and $\langle q \rangle$ is the averaged Bader charges on the oxygen sublattice. Fig. 6 shows the charge delocalization over the oxygen sublattice for each Sc fraction considered here. The trend clearly shows that there is a marked increase in charge delocalization with Sc content which corresponds to lower vacancy formation energies as shown in Fig. 5(a). This differs from the undoped case of $SrCoO_3$ where the two electrons tend to localize on neighbouring Co sites.[35]

It has been shown that the vacancy formation energy correlates with the p-band centre, such that either of which could be used as an activity descriptor [16,52]. This correlation also holds for the structures considered here. The p-band centre for $SrScO_3$ is -0.63 eV whereas in SrCoO3 and $SrNbO_3$ it is found to be -1.92 eV and -4.40 relative to the Fermi level, respectively. Grimaud et al. [16] have argued that moving the p-band centre close to the Fermi level can increase the OER activity but having it too close will decrease the oxide stability. For this reason BSCF which has its p-band centre at ~ -1.5 eV exhibits low OER overpotentials but readily amorphizes leading to a drop in activity.

The recent demonstration that Sc and Nb additives to $SrCoO_3$ help achieve high OER activity can therefore be understood based on the fact that small fractions of Sc and Nb help stabilize the cubic structure by preserving the cubic perovskite structure as well as the electronic structure of $SrCoO_3$. The increased oxygen vacancy formation energy for low Sc and Nb doping fractions maintains a near stoichiometric concentration of oxygen ions. Our earlier work has revealed a detrimental role of surface oxygen vacancies on the OER activity in $SrCoO_3$ [35]. Hence, minimizing oxygen vacancy concentrations can be expected to help minimize the overpotential for OER. Sc on the other hand helps move the p-band centre close to the Fermi level (Fig. 5(d)) which contributes to the OER activity and offsets the effect of

Nb which tends to shift the p-band centre in the opposite direction. However, at x = 0.222 the p-band centre is already at ~-1.7 eV relative to the Fermi level and is therefore at the edge of materials stability [16]. On the other hand, increasing the Sc fraction clearly leads to a significant increase in oxygen vacancy concentration and would therefore be beneficial in SOFCs. This is in very good agreement with earlier experimental studies [53,54] where it was demonstrated that Sc additives in $SrCoO_3$ did lead to an extremely high oxygen vacancy concentration and an improved performance as a cathode material.

Conclusions

In summary, we have examined Sc and Nb dopant distributions in $SrCoO_3$. We have shown that $SrScO_3$ exhibits a high degree of electronic instability due to the presence of a significant contribution of antibonding states below the Fermi level. Sc additives lead to a lattice expansion and within the doping fractions considered here Vegard's law is obeyed.

Oxygen vacancies in the vicinity of Nb ions have large formation energies relative to vacancies in bulk $SrCoO_3$. This makes Nb efficient in preserving oxygen stoichiometry as it acts as oxygen traps. On the other hand, increasing Sc concentration introduces electronic instabilities as revealed from the COHP analysis which drives the vacancies formation to lower values. The p-band centre of $SrCoO_3$ at -1.92 eV can be further tuned by the dopants. We find that Sc has a tendency to shift p-band centre closer to the Fermi level. However, the expected amorphization in the doped structures and the increased oxygen vacancies means that increasing the Sc content is not ideal for OER operations. Our analysis sheds light at the origin of the high oxygen vacancy concentration induced by Sc at larger doping percentages which helps explain the successful demonstration of Sc doped $SrCoO_3$ as a cathode in fuel cells [53,54].

ACKNOWLEDGEMENT

This research was undertaken with the assistance of UNSW Australia SPF01 funding (SCS). We acknowledge generous allocations of supercomputing time at the Pawsey Supercomputing Centre via the Australian National Computational Merit Allocation Scheme (NCMAS project fr2) and the Energy and Resources Merit Allocation Scheme of the Pawsey Supercomputing Centre (project pawsey0111). Additional computational resources were provided by KAUST on the Shaheen II supercomputer.

References

[1] W.T. Hong, M. Risch, K.A. Stoerzinger, A. Grimaud, J. Suntivich, Y. Shao-Horn, Toward the rational design of non-precious transition metal oxides for oxygen electrocatalysis, Energy Environ. Sci. 8 (2015) 1404–1427.

[2] I. Katsounaros, S. Cherevko, A.R. Zeradjanin, K.J.J. Mayrhofer, Oxygen Electrochemistry as a Cornerstone for Sustainable Energy Conversion, Angew. Chemie Int. Ed. 53 (2014) 102–121.

[3] Y. Matsumoto, E. Sato, Electrocatalytic properties of transition metal oxides for oxygen evolution reaction, Mater. Chem. Phys. 14 (1986) 397–426.

[4] J. Suntivich, H. a Gasteiger, N. Yabuuchi, H. Nakanishi, J.B. Goodenough, Y. Shao-

Horn, Design principles for oxygen-reduction activity on perovskite oxide catalysts for fuel cells and metal–air batteries, Nat. Chem. 3 (2011) 546–550.

[5] J. Chakhalian, a. J. Millis, J. Rondinelli, Whither the oxide interface, Nat. Mater. 11 (2012) 92–94. doi:10.1038/nmat3225.

[6] A. Chroneos, B. Yildiz, A. Tarancón, D. Parfitt, J. a. Kilner, Oxygen diffusion in solid oxide fuel cell cathode and electrolyte materials: mechanistic insights from atomistic simulations, Energy Environ. Sci. 4 (2011) 2774.

[7] P. Bezdicka, A. Wattiaux, J.C. Grenier, M. Pouchard, P. Hagenmuller, Preparation and characterization of Fully stoichiometric SrCoO3 by electrochemical oxidation, Zeitschrift Für Anorg. Und Allg. Chemie. 619 (1993) 7–12.

[8] H. Jeen, W.S. Choi, M.D. Biegalski, C.M. Folkman, I.-C. Tung, D.D. Fong, J.W. Freeland, D. Shin, H. Ohta, M.F. Chisholm, H.N. Lee, Reversible redox reactions in an epitaxially stabilized $SrCoO_x$ oxygen sponge, Nat. Mater. 12 (2013) 1057–1063.

[9] H. Jeen, Z. Bi, W.S. Choi, M.F. Chisholm, C. a. Bridges, M.P. Paranthaman, H.N. Lee, Orienting Oxygen Vacancies for Fast Catalytic Reaction, Adv. Mater. 25 (2013) 6459–6463.

[10] Z. Wang, R. Peng, W. Zhang, X. Wu, C. Xia, Y. Lu, Oxygen reduction and transport on the $La_{1-x}Sr_xCo_{1-y}Fe_yO_{3-\delta}$ cathode in solid oxide fuel cells: a first-principles study, J. Mater. Chem. A. 1 (2013) 12932.

[11] Y. Matsumoto, Oxygen Evolution on $La_{1-x}Sr_xCoO_3$ Electrodes in Alkaline Solutions, J. Electrochem. Soc. 127 (1980) 811.

[12] Z. Shao, S.M. Haile, A high-performance cathode for the next generation of solid-

oxide fuel cells, Nature. 431 (2004) 170–173.

[13] F. Baumann, J. Fleig, H. Habermeier, J. Maier, $Ba_{0.5}Sr_{0.5}Co_{0.8}Fe_{0.2}O_{3-\delta}$ thin film microelectrodes investigated by impedance spectroscopy, Solid State Ionics. 177 (2006) 3187–3191.

[14] C. Zhang, P.D. Bristowe, First principles calculations of oxygen vacancy formation in barium-strontium-cobalt-ferrite, Rsc Adv. 3 (2013) 12267–12274.

[15] J. Suntivich, K.J. May, H.A. Gasteiger, J.B. Goodenough, Y. Shao-Horn, A Perovskite Oxide Optimized for Oxygen Evolution Catalysis from Molecular Orbital Principles, Science. 334 (2011) 1383–1385.

[16] A. Grimaud, K.J. May, C.E. Carlton, Y.-L. Lee, M. Risch, W.T. Hong, J. Zhou, Y. Shao-Horn, Double perovskites as a family of highly active catalysts for oxygen evolution in alkaline solution, Nat. Commun. 4 (2013) 2439.

[17] M.M. Kuklja, Y.A. Mastrikov, B. Jansang, E. a. Kotomin, First principles calculations of (Ba,Sr)(Co,Fe)$O_{3-\delta}$ structural stability, Solid State Ionics. 230 (2013) 21–26.

[18] I.C. Man, H.-Y. Su, F. Calle-Vallejo, H. a. Hansen, J.I. Martínez, N.G. Inoglu, J. Kitchin, T.F. Jaramillo, J.K. Nørskov, J. Rossmeisl, Universality in Oxygen Evolution Electrocatalysis on Oxide Surfaces, ChemCatChem. 3 (2011) 1159–1165.

[19] F. Calle-Vallejo, O.A. Díaz-Morales, M.J. Kolb, M.T.M. Koper, Why Is Bulk Thermochemistry a Good Descriptor for the Electrocatalytic Activity of Transition Metal Oxides?, ACS Catal. 5 (2015) 869–873.

[20] X. Cheng, E. Fabbri, M. Nachtegaal, I.E. Castelli, M. El Kazzi, R. Haumont, N. Marzari, T.J. Schmidt, Oxygen Evolution Reaction on $La_{1-x}Sr_xCoO_3$ Perovskites: A

Combined Experimental and Theoretical Study of Their Structural, Electronic, and Electrochemical Properties, Chem. Mater. 27 (2015) 7662–7672.

[21] G. Kresse, J. Furthmüller, Efficient iterative schemes for ab initio total-energy calculations using a plane-wave basis set, Phys. Rev. B. 54 (1996) 11169–11186.

[22] G. Kresse, D. Joubert, From ultrasoft pseudopotentials to the projector augmented-wave method, Phys. Rev. B. 59 (1999) 1758–1775.

[23] J.P. Perdew, A. Ruzsinszky, G.I. Csonka, O.A. Vydrov, G.E. Scuseria, L.A. Constantin, X. Zhou, K. Burke, Restoring the Density-Gradient Expansion for Exchange in Solids and Surfaces, Phys. Rev. Lett. 100 (2008) 136406.

[24] J. Young, J.M. Rondinelli, Crystal structure and electronic properties of bulk and thin film brownmillerite oxides, Phys. Rev. B. 92 (2015) 174111.

[25] P. V. Balachandran, D. Puggioni, J.M. Rondinelli, Crystal-Chemistry Guidelines for Noncentrosymmetric A_2BO_4 Ruddlesden−Popper Oxides, Inorg. Chem. 53 (2014) 336–348.

[26] K.H.L. Zhang, Y. Du, P. V Sushko, M.E. Bowden, V. Shutthanandan, L. Qiao, G.X. Cao, Z. Gai, S. Sallis, L.F.J. Piper, S. a Chambers, Electronic and magnetic properties of epitaxial perovskite $SrCrO_3$(001), J. Phys. Condens. Matter. 27 (2015) 245605.

[27] A. Walsh, D.O. Scanlon, S. Chen, X.G. Gong, S.-H. Wei, Self-Regulation Mechanism for Charged Point Defects in Hybrid Halide Perovskites, Angew. Chemie Int. Ed. 54 (2015) 1791–1794.

[28] A. van de Walle, P. Tiwary, M. de Jong, D.L. Olmsted, M. Asta, A. Dick, D. Shin, Y. Wang, L.-Q. Chen, Z.-K. Liu, Efficient stochastic generation of special quasirandom

structures, Calphad. 42 (2013) 13–18.

[29] H. Wang, a Chroneos, C. Jiang, U. Schwingenschlögl, Special quasirandom structures for gadolinia-doped ceria and related materials., Phys. Chem. Chem. Phys. 14 (2012) 11737–42.

[30] H. Wang, A. Chroneos, C. Jiang, U. Schwingenschlogl, Modelling zirconium hydrides using the special quasirandom structure approach, Phys. Chem. Chem. Phys. 15 (2013) 7599–7603.

[31] A.M. Ritzmann, A.B. Muñoz-García, M. Pavone, J.A. Keith, E.A. Carter, Ab Initio DFT+U Analysis of Oxygen Vacancy Formation and Migration in $La_{1-x}Sr_xFeO_{3-\delta}$ (x = 0, 0.25, 0.50), Chem. Mater. 25 (2013) 3011–3019.

[32] A.M. Ritzmann, J.M. Dieterich, E.A. Carter, Density functional theory + U analysis of the electronic structure and defect chemistry of LSCF ($La_{0.5}Sr_{0.5}Co_{0.25}Fe_{0.75}O_{3-\delta}$), Phys. Chem. Chem. Phys. 18 (2016) 12260–12269.

[33] S. Maintz, V.L. Deringer, A.L. Tchougréeff, R. Dronskowski, Analytic projection from plane-wave and PAW wavefunctions and application to chemical-bonding analysis in solids, J. Comput. Chem. 34 (2013) 2557–2567.

[34] S. Maintz, V.L. Deringer, A.L. Tchougréeff, R. Dronskowski, LOBSTER: A tool to extract chemical bonding from plane-wave based DFT, J. Comput. Chem. 37 (2016) 1030–1035.

[35] H.A. Tahini, X. Tan, U. Schwingenschlögl, S.C. Smith, Formation and Migration of Oxygen Vacancies in SrCoO 3 and Their Effect on Oxygen Evolution Reactions, ACS Catal. 6 (2016) 5565–5570.

[36] W. Zhou, M. Zhao, F. Liang, S.C. Smith, Z. Zhu, High activity and durability of novel perovskite electrocatalysts for water oxidation, Mater. Horiz. 2 (2015) 495–501.

[37] P. Zeng, R. Ran, Z. Chen, W. Zhou, H. Gu, Z. Shao, S. Liu, Efficient stabilization of cubic perovskite $SrCoO_{3-\delta}$ by B-site low concentration scandium doping combined with sol–gel synthesis, J. Alloys Compd. 455 (2008) 465–470.

[38] D. Chen, C. Chen, Z. Zhang, Z.M. Baiyee, F. Ciucci, Z. Shao, Compositional Engineering of Perovskite Oxides for Highly Efficient Oxygen Reduction Reactions, ACS Appl. Mater. Interfaces. 7 (2015) 8562–8571.

[39] G. Henkelman, A. Arnaldsson, H. Jónsson, A fast and robust algorithm for Bader decomposition of charge density, Comput. Mater. Sci. 36 (2006) 354–360.

[40] E. a. Kotomin, Y. a. Mastrikov, M.M. Kuklja, R. Merkle, A. Roytburd, J. Maier, First principles calculations of oxygen vacancy formation and migration in mixed conducting $Ba_{0.5}Sr_{0.5}Co_{1-y}Fe_yO_{3-\delta}$ perovskites, Solid State Ionics. 188 (2011) 1–5.

[41] A.M. Ritzmann, M. Pavone, A.B. Muñoz-García, J.A. Keith, E.A. Carter, Ab initio DFT+U analysis of oxygen transport in $LaCoO_3$: the effect of Co^{3+} magnetic states, J. Mater. Chem. A. 2 (2014) 8060–8074.

[42] Y.A. Mastrikov, M.M. Kuklja, E.A. Kotomin, J. Maier, First-principles modelling of complex perovskite $(Ba_{1-x}Sr_x)(Co_{1-y}Fe_y)O_{3-\delta}$ for solid oxide fuel cell and gas separation membrane applications, Energy Environ. Sci. 3 (2010) 1544.

[43] L. Wang, T. Maxisch, G. Ceder, Oxidation energies of transition metal oxides within the GGA+U framework, Phys. Rev. B. 73 (2006) 195107.

[44] Y.-L. Lee, J. Kleis, J. Rossmeisl, D. Morgan, Ab initio energetics of $LaBO_3$(001) (B =

Mn , Fe, Co, and Ni) for solid oxide fuel cell cathodes, Phys. Rev. B. 80 (2009) 224101.

[45] T. a. Mellan, K.P. Maenetja, P.E. Ngoepe, S.M. Woodley, C.R. a. Catlow, R. Grau-Crespo, Lithium and oxygen adsorption at the β-MnO_2 (110) surface, J. Mater. Chem. A. 1 (2013) 14879.

[46] I.T. Todorov, N.L. Allan, M.Y. Lavrentiev, C.L. Freeman, C.E. Mohn, J. a Purton, Simulation of mineral solid solutions at zero and high pressure using lattice statics, lattice dynamics and Monte Carlo methods, J. Phys. Condens. Matter. 16 (2004) S2751–S2770.

[47] K. Zhang, R. Ran, L. Ge, Z. Shao, W. Jin, N. Xu, Systematic investigation on new $SrCo_{1-y}Nb_yO_{3-\delta}$ ceramic membranes with high oxygen semi-permeability, J. Memb. Sci. 323 (2008) 436–443.

[48] S. Zhang, N. Han, X. Tan, Density functional theory calculations of atomic, electronic and thermodynamic properties of cubic LaCoO 3 and $La_{1-x}Sr_xCoO_3$ surfaces, RSC Adv. 5 (2015) 760–769.

[49] D. Lee, Y.-L. Lee, W.T. Hong, M.D. Biegalski, D. Morgan, Y. Shao-Horn, Oxygen surface exchange kinetics and stability of $(La,Sr)_2CoO_{4\pm\delta}/La_{1-x}Sr_xMO_{3-\delta}$ (M = Co and Fe) hetero-interfaces at intermediate temperatures, J. Mater. Chem. A. 3 (2015) 2144–2157.

[50] A.B. Muñoz-García, A.M. Ritzmann, M. Pavone, J.A. Keith, E.A. Carter, Oxygen Transport in Perovskite-Type Solid Oxide Fuel Cell Materials: Insights from Quantum Mechanics, Acc. Chem. Res. 47 (2014) 3340–3348.

[51] M. Pavone, A.B. Muñoz-García, A.M. Ritzmann, E.A. Carter, First-Principles Study

of Lanthanum Strontium Manganite: Insights into Electronic Structure and Oxygen Vacancy Formation, J. Phys. Chem. C. 118 (2014) 13346–13356.

[52] Y.-L. Lee, J. Kleis, J. Rossmeisl, Y. Shao-Horn, D. Morgan, Prediction of solid oxide fuel cell cathode activity with first-principles descriptors, Energy Environ. Sci. 4 (2011) 3966.

[53] W. Zhou, Z. Shao, R. Ran, R. Cai, Novel $SrSc_{0.2}Co_{0.8}O_{3-\delta}$ as a cathode material for low temperature solid-oxide fuel cell, Electrochem. Commun. 10 (2008) 1647–1651.

[54] W. Zhou, B. An, R. Ran, Z. Shao, Electrochemical Performance of $SrSc_{0.2}Co_{0.8}O_{3-\delta}$ Cathode on $Sm_{0.2}Ce_{0.8}O_{1.9}$ Electrolyte for Low Temperature SOFCs, J. Electrochem. Soc. 156 (2009) B884.

TOC